Remote Sensing of Environment 148 (2014) 108–118

Contents lists available at ScienceDirect

Remote Sensing of Environment

journal homepage: www.elsevier.com/locate/rse

A MODIS-based Photosynthetic Capacity Model to estimate gross primary production in Northern China and the Tibetan Plateau

Yanni Gao [a,b], Guirui Yu [a,*], Huimin Yan [a], Xianjin Zhu [a,b], Shenggong Li [a], Qiufeng Wang [a], Junhui Zhang [c], Yanfen Wang [b], Yingnian Li [d], Liang Zhao [d], Peili Shi [a]

[a] Synthesis Research Center of Chinese Ecosystem Research Network, Key Laboratory of Ecosystem Network Observation and Modeling, Institute of Geographic Sciences and Natural Resources Research, Chinese Academy of Sciences, Beijing 100101, China
[b] University of Chinese Academy of Sciences, Beijing, 100049, China
[c] Institute of Applied Ecology, Chinese Academy of Sciences, Shenyang, 110016, China
[d] Northwest Institute of Plateau Biology, Chinese Academy of Sciences, Xining, 810001, China

ARTICLE INFO

Article history:
Received 14 July 2013
Received in revised form 8 January 2014
Accepted 1 March 2014
Available online 16 April 2014

Keywords:
Gross primary production (GPP)
Eddy covariance
Vegetation index
Moisture index
Photosynthetic capacity
Photosynthetic Capacity Model (PCM)

ABSTRACT

Accurate quantification of the spatio-temporal variation of gross primary production (GPP) for terrestrial ecosystems is significant for ecosystem management and the study of the global carbon cycle. In this study, we propose a MODIS-based Photosynthetic Capacity Model (PCM) to estimate GPP in Northern China and the Tibetan Plateau. The PCM follows the logic of the light use efficiency model and is only driven by the Enhanced Vegetation Index (EVI) and the Land Surface Water Index (LSWI). Multi-year eddy CO_2 flux data from five vegetation types in North China (temperate mixed forest, temperate steppe) and the Tibetan Plateau (alpine shrubland, alpine marsh and alpine meadow-steppe) were used for model parameterization and validation. In most cases, the seasonal and interannual variation in the simulated GPP agreed well with the observed GPP. Model comparisons showed that the predictive accuracy of the PCM was higher than that of the MODIS GPP products and was comparable with that of the Vegetation Photosynthesis Model (VPM) and the potential PAR-based GPP models. The model parameter (PC_{max}) of the PCM represents the maximum photosynthetic capacity, which showed a good linear relationship with the mean annual nighttime Land Surface Temperature (LST_{an}). With this linear function, the PCM-simulated GPP can explain approximately 93% of the variation in the flux-observed GPP across all five vegetation types. These analyses demonstrated the potential of the PCM as an alternative tool for regional GPP estimation.

© 2014 Elsevier Inc. All rights reserved.

1. Introduction

Gross primary production (GPP) is defined as the photosynthetic rate at which plants capture and store chemical energy in a given length of time (Chapin, Matson, & Vitousek, 2011, Chap. 5). GPP is the first step in the input of atmospheric CO_2 to terrestrial ecosystems (vegetation and the soil) and a key component of the carbon biogeochemical cycle that links atmospheric CO_2 and terrestrial ecosystems (Yuan et al., 2010). Quantifying GPP at regional and global scales is essential to the understanding of the carbon cycle of terrestrial ecosystems (Beer et al., 2010; Gitelson et al., 2006; Yu et al., 2006, 2013).

The eddy covariance (EC) technique instantaneously measures the net ecosystem exchange of CO_2 (NEE) between terrestrial ecosystems and the atmosphere. Its long-term network observations provide valuable information for developing and validating GPP models (Yu et al., 2006; Yuan et al., 2007). Remote sensing (RS) technology repeatedly monitors dynamic changes in terrestrial ecosystem structure and functions at a high temporal–spatial resolution. Its continuous observations play an increasing role in estimating GPP at regional and global scales (Prince & Goward, 1995; Xiao, Hollinger, et al., 2004). Incorporating both EC flux data and RS imagery, many satellite-based GPP models have been developed, e.g., the Vegetation Photosynthesis Model (VPM, Xiao, Hollinger, et al., 2004), the MODIS GPP algorithm (Running et al., 2004), the EC–LUE model (Yuan et al., 2007), the Temperature and Greenness model (TG, Sims et al., 2008), the Vegetation Index model (VI, Wu, Munger, Niu, & Kuang, 2010) and the Greenness and Radiation model (GR, Gitelson et al., 2006, 2012; Peng, Gitelson, Keydan, Rundquist, & Moses, 2011; Peng, Gitelson, & Sakamoto, 2013; Sakamoto, Gitelson, Wardlow, Verma, & Suyker, 2011; Wu, Chen, & Huang, 2011).

Most satellite-based GPP models have been based on the theory of light use efficiency proposed by Monteith (1972, 1977), who suggested that crop productivity is strongly related to the intercepted solar radiation and thus can be estimated as the product of the intercepted solar radiation and its conversion efficiency into plant photosynthate, i.e., light use efficiency (LUE). Based on the method used to estimate

* Corresponding author at: Institute of Geographic Sciences and Natural Resources Research, Chinese Academy of Sciences, 11A Datun Road, Chaoyang District, Beijing 100101, China. Tel.: +86 10 64889432.
E-mail address: yugr@igsnrr.ac.cn (G. Yu).

http://dx.doi.org/10.1016/j.rse.2014.03.006
0034-4257/© 2014 Elsevier Inc. All rights reserved.

LUE, these satellite-based GPP models can be classified into two categories. The first category includes those models that employ biome-dependent or biome-independent maximum light use efficiency to calculate LUE, e.g., VPM, the MODIS GPP algorithm and EC–LUE. The general formula for models of this type is as follows:

$$\mathrm{GPP} = \varepsilon_{\max} \times f \times \mathrm{FPAR} \times \mathrm{PAR}, \quad (1)$$

where PAR is the incident photosynthetically active radiation (mol PPFD m^{-2} s^{-1} or mol PPFD m^{-2} d^{-1}), FPAR is the fraction of PAR absorbed by the plant canopy, the product of FPAR and PAR is the PAR absorbed by the plant canopy (APAR), $\varepsilon_{\max}$ is the maximum LUE without environmental stresses (mol C mol $APAR^{-1}$) and f is a downward regulating factor for $\varepsilon_{\max}$ ranging from 0 to 1 under various environmental limiting conditions. Thus, the product of $\varepsilon_{\max}$ and f is the actual LUE. Factor f is usually a function of temperature (T), soil moisture (SM) and/or water vapor pressure deficit (VPD),

$$f = f_T \times f_{SM} \times f_{VPD}. \quad (2)$$

Models of this type may differ in their approach to estimate $\varepsilon_{\max}$ and f in Eq. (1). For example, the VPM obtains biome-specific $\varepsilon_{\max}$ from the literature or from the relationship between NEE and incident PAR. The f of this model includes air temperature (T_a), land surface water conditions and phenology (Xiao, Hollinger, et al., 2004). The MODIS GPP algorithm uses biome-specific $\varepsilon_{\max}$ from biome parameter lookup tables, and the low temperature and high VPD are chosen to down-regulate $\varepsilon_{\max}$ (Running et al., 2004). The EC–LUE model sets an invariant $\varepsilon_{\max}$ across all biomes, and f equals the minimum value of scalars for the respective effects of T_a and soil moisture on $\varepsilon_{\max}$ according to Liebig's law (Yuan et al., 2007).

The second category of GPP models, such as TG, VI and GR, involves simplified versions of Eq. (1) based on the relationships between remote sensing data and key factors affecting photosynthesis. Models of this category differ according to the simplified factors. For example, because there are good relationships between Land Surface Temperature (LST) and T_a, VPD and PAR, the TG model is solely driven by LST and the Enhanced Vegetation Index (EVI) from MODIS imagery (Sims et al., 2008). Because the vegetation index is a reliable proxy for both LUE and FPAR, the VI model simply takes the form of GPP ∝ EVI ×EVI × PAR (Wu, Munger, et al., 2010). It has been reported that both GPP and the vegetation index have close relationships with canopy chlorophyll content. Thus, the GR model estimates GPP based on the product of the vegetation index and either incident PAR or potential PAR (Gitelson et al., 2006, 2012; Peng et al., 2011, 2013; Sakamoto et al., 2011; Wu et al., 2011).

The first category of GPP models requires ground meteorological observations as input variables. These observations usually have insufficiently detailed temporal and spatial resolution and introduce simulation errors into the outputs for large areas (Rahman, Sims, Cordova, & El-Masri, 2005; Sims et al., 2006, 2008). The GPP models in the second category reduce or avoid their dependence on ground meteorological observations. These features promote their application at regional and global scales. However, the ecological meaning of the model parameters is not nearly as clear as that of the parameters in the first category of GPP models (Yang, Shang, Guan, & Jiang, 2013). Accordingly, the principal goal of this paper is to develop an entirely satellite-based GPP model in which the model parameter has a clear ecological meaning. The specific objectives are as follows: (1) to apply the flux data from five vegetation types in North China and the Tibetan Plateau to parameterize and validate the model, (2) to explore the possibility of using remote sensing data to simulate the spatial variation in the model parameter, (3) to analyze the seasonal and inter-seasonal dynamics of the simulated GPP and (4) to compare the predictive accuracy of the PCM with that of the MODIS GPP products and the VPM.

2. Model description

2.1. Model structure

According to Monteith's (1972, 1977) logic, incident PAR (inPAR) is the energy source for photosynthesis and is included as an important variable in LUE models. Over short time periods (minutes to hours), photosynthesis increases with the increase in inPAR under light-limited conditions. When inPAR exceeds what plants need, photosynthesis begins to saturate and then tends to decrease (e.g., Alton, North, & Los, 2007; Ibrom et al., 2008; Lagergren et al., 2005; Propastin, Ibrom, Knohl, & Erasmi, 2012; Sims et al., 2005; Turner et al., 2003; Zhang et al., 2011). In contrast to the results on an hourly time scale, daily inPAR has a very weak relationship with daily gross photosynthesis within many types of ecosystems, even during the peak growing season, when inPAR has the strongest direct effect on photosynthesis (Sims et al., 2005). The daily inPAR in the Arctic is nearly the same as that in the tropics during midsummer; however, the tropics have a greater daily carbon gain than the Arctic (Chapin et al., 2011, Chap. 5). The annual inPAR also has no relationship with annual GPP across biomes from tundra to rainforest (Garbulsky et al., 2010).

It was reported that inPAR can introduce unpredictable uncertainty in GPP estimation for crops due to variable atmospheric conditions such as clouds, aerosols and water vapor (Gitelson et al., 2012; Peng et al., 2013). Potential PAR (pPAR) can be considered as the maximal value of inPAR that may occur when the concentrations of atmospheric aerosols and gases are minimal, which excludes the frequent fluctuations in inPAR and has been shown to perform more satisfactorily than inPAR in GPP estimation for crops (Gitelson et al., 2012; Peng et al., 2013). The likely reason for this outcome is that the acclimation and adaptation mechanisms of plants to unfavorable light conditions can maximize light absorption and minimize light damage by adjusting their physiological and genetic features (e.g., Chapin et al., 2011, Chap. 5; Ehleringer, Björkman, & Mooney, 1976; Koller, 2000; Taiz & Zeiger, 2002, Chap. 9). The pPAR during the growing season can be expressed as the product of the maximum pPAR ($\mathrm{pPAR_{max}}$, mol PPFD m^{-2} d^{-1}) and a down-regulated factor that varies with the day of a year ($\mathrm{pPAR_t}$). If we use pPAR in place of inPAR in Eq. (1), we obtain the following result:

$$\mathrm{GPP} = (\varepsilon_{\max} \times \mathrm{pPAR_{max}}) \times (\mathrm{FPAR} \times \mathrm{pPAR_t}) \times f. \quad (3)$$

The product of $\varepsilon_{\max}$ and $\mathrm{pPAR_{max}}$ represents the maximum photosynthetic capacity (termed $PC_{\max}$, mol C m^{-2} d^{-1}), and the product of FPAR and $\mathrm{pPAR_t}$ is a down-regulated factor that varies with the absorbed PAR, which can be used to represent the variability of photosynthetic capacity under different growth stages (PC_t). Photosynthetic capacity is defined as the photosynthetic rate under favorable environmental conditions (Chapin et al., 2011, Chap. 5). Thus, the LUE model can be converted into the following model based on the concept of photosynthetic capacity:

$$\mathrm{GPP} = PC_{\max} \times PC_t \times f. \quad (4)$$

This equation specifies the general form of our developed GPP model, termed the Photosynthetic Capacity Model (PCM). Photosynthetic capacity depends on the amount of photosynthetic apparatus within a plant community and can be directly expressed by the total content of canopy chlorophyll (Gitelson, Viña, Ciganda, Rundquist, & Arkebauer, 2005; Medina & Lieth, 1964; Muraoka & Koizumi, 2005; Peng et al., 2011; Schlemmer et al., 2013; Whittaker & Marks, 1975). A number of studies have explored methods of estimating canopy chlorophyll content from vegetation indices. Such estimation has been shown to be feasible and can provide acceptable accuracy (Gitelson et al., 2005; Hunt et al., 2013). EVI has been reported to show close correlations with chlorophyll content at both the leaf and the canopy levels (Huang et al.,

Table 1
Brief description of the five vegetation types.

Vegetation type	Site name	Code	Latitude	Longitude	Mean annual temperature (°C)	Mean annual precipitation (mm)	Data available period	Reference
Broad-leaved Korean pine mixed forest	Changbaishan	CBS	42.40	128.10	0.9–4.0	600–810	2003–2008	Zhang et al. (2009)
Temperate steppe	Inner Mongolia	NM	43.55	116.68	−0.4	350.9	2004–2008	Wu et al. (2008)
Alpine shrubland	Haibei	HBGC	37.67	101.33	−1.7	600	2004–2011	Li et al. (2007)
Alpine marsh	Haibei	HBSD	37.61	101.31	−1.7	600	2004–2008	Li et al. (2007)
Alpine meadow-steppe	Damxung	DX	30.85	91.08	1.3	480	2004–2009	Fu et al. (2009)

2012; Ide, Nakaji, & Oguma, 2010; Muraoka et al., 2013; Nagai, Saigusa, Muraoka, & Nasahara, 2010; Wu, Munger, et al., 2010). Biophysical research has also indicated that EVI is sensitive to canopy variations and is barely saturated in multi-layered and closed canopies (Huete et al., 2002; Xiao, Hollinger, et al., 2004). Because EVI is readily obtained at high temporal and spatial resolution from satellite imagery, it is used to represent the variability of photosynthetic capacity in this version of the PCM.

Under actual environmental conditions, photosynthesis is limited by environmental stress. It has been reported that moisture is a key factor controlling plant photosynthesis, e.g., in semidesert grassland in southeastern Arizona, USA (Scott, Hamerlynck, Jenerette, Moran, & Barron-Gafford, 2010) and in savanna in Africa (Sjöström et al., 2011). Research at 28 AmeriFlux and EuroFlux sites, including five major terrestrial biomes (deciduous broadleaf forest, mixed forest, evergreen needleleaf forest, grassland and savanna), has indicated that moisture conditions control photosynthesis at most sites except at the beginning and end of the growing season when temperature controls photosynthesis in certain ecosystems (Yuan et al., 2007). Phenological studies have indicated that the accumulated temperature above a certain threshold agrees well with the timing of bud burst in boreal ecosystems (Linkosalo, 2000); in temperate Eastern China, the spatial patterns of the mean spring and autumn air temperatures were significantly correlated with those of the beginning and ending dates of the growing season, respectively (Chen, Hu, & Yu, 2005). This relationship between temperature and photosynthesis at the beginning and end of the growing season can also be represented appropriately by an EVI time series (Zhang et al., 2003).

Soil moisture is the source of water for plant growth, and VPD indicates the evaporative demand in the atmosphere. Plant photosynthesis depends primarily on the dynamics of both soil moisture and VPD (Xiao, Hollinger, et al., 2004). A number of light use efficiency models use soil moisture and/or VPD to mirror the effect of moisture conditions on photosynthesis (Potter et al., 1993; Prince & Goward, 1995; Running et al., 2004). However, it is difficult to quantify soil moisture across large areas based on either remote sensing or modeling, and this difficulty limits the spatial application of soil-moisture dependent models (Yuan et al., 2007). The VPM developed a moisture index (W_{scalar}) as an alternative to represent the dynamic change of canopy water content (Xiao, Hollinger, et al., 2004). W_{scalar} has been successfully applied in GPP estimation in many ecosystems, e.g., evergreen needleleaf forest (Xiao, Hollinger, et al., 2004), deciduous broadleaf forest (Xiao, Zhang, et al., 2004), tropical evergreen forest (Xiao et al., 2005), cropland (Kalfas, Xiao, Vanegas, Verma, & Suyker, 2011; Yan et al., 2009), grassland (Wu et al., 2008), shrubland (Li et al., 2007) and wetland (Li et al., 2007). Because W_{scalar} can also be calculated from easily obtained remote sensing data, it is used to represent the seasonal variation of canopy water content in this version of the PCM.

2.2. Model algorithms

From the above specifications, the PCM can be expressed as follows:

$$\mathrm{GPP} = PC_{\max} \times \mathrm{EVI_s} \times W_s, \tag{5}$$

where PC_{max} stands for the maximum photosynthetic capacity for a certain region (e.g., mol C m^{-2} d^{-1}), EVI_s represents the variability of photosynthetic capacity and W_s indicates the moisture conditions that downward regulate photosynthetic capacity. The values of EVI_s and W_s are set to zero before and after the growing season, when photosynthesis does not occur. The beginning and end of the growing season are identified from the EVI time series (Zhang et al., 2003).

Because GPP is almost 0 when EVI is approximately 0.1 (Sims et al., 2006), the equation developed for the TG model is used as follows to represent the variability of photosynthetic capacity (Sims et al., 2008):

$$\mathrm{EVI_s} = \mathrm{EVI} - 0.1. \tag{6}$$

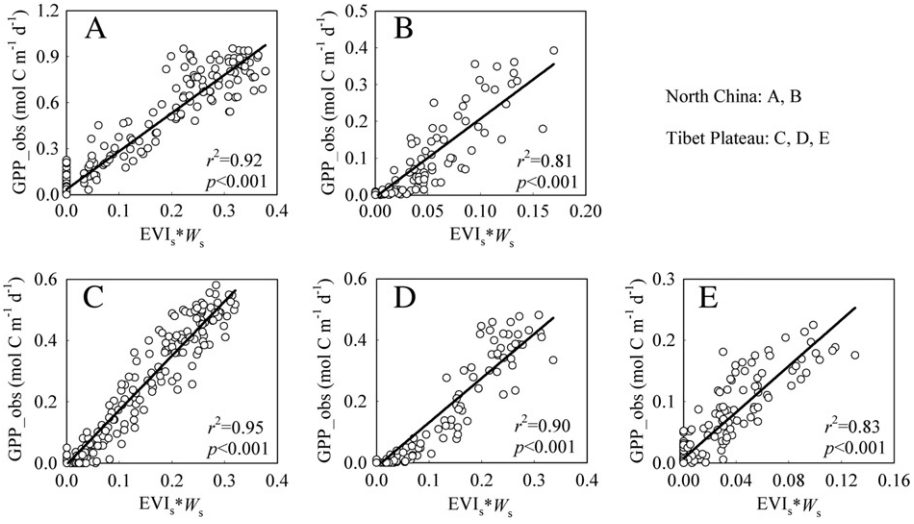

Fig. 1. The relationship between the observed GPP and $EVI_s \times W_s$, based on an 8-day average. W_s: moisture index. A: temperate mixed forest (CBS), B: temperate steppe (NM), C: alpine shrubland (HBGC), D: alpine marsh (HBSD), and E: alpine meadow-steppe (DX).

The EVI is computed from the following equation (Huete et al., 2002):

$$\mathrm{EVI} = G \times \frac{\rho_{\mathrm{nir}} - \rho_{\mathrm{red}}}{\rho_{\mathrm{nir}} + (C_1 \times \rho_{\mathrm{red}} - C_2 \times \rho_{\mathrm{blue}}) + L}, \quad (7)$$

where $G = 2.5$, $C_1 = 6.0$, $C_2 = 7.5$, $L = 1$ and ρ_{nir}, ρ_{red} and ρ_{blue} are the spectral reflectances of the near infrared, red, and blue bands in MODIS imagery, respectively (Huete et al., 2002).

The W_s is modified as follows from the equation for W_{scalar} (Xiao, Hollinger, et al., 2004):

$$W_{\mathrm{scalar}} = \frac{1 + \mathrm{LSWI}}{1 + \mathrm{LSWI}_{\mathrm{max}}}, \quad (8)$$

where LSWI is the Land Surface Water Index and $\mathrm{LSWI}_{\mathrm{max}}$ is the maximum LSWI during the growing season for each pixel (Xiao, Hollinger, et al., 2004). Because the values of W_{scalar} depend upon $\mathrm{LSWI}_{\mathrm{max}}$, there may be similar or identical W_{scalar} values under different vegetation types even though their actual canopy water content varies considerably. Thus, W_{scalar} can represent a temporal dynamic but spatial pattern of moisture conditions. In this version of the PCM, $\mathrm{LSWI}_{\mathrm{max}}$ was assumed to be 1 to allow spatial comparison. The modified equation for W_{scalar}, i.e., W_s, is capable of representing both temporal and spatial variation in moisture conditions.

The equation for LSWI is as follows (Xiao, Hollinger, et al., 2004):

$$\mathrm{LSWI} = \frac{\rho_{\mathrm{nir}} - \rho_{\mathrm{swir}}}{\rho_{\mathrm{nir}} + \rho_{\mathrm{swir}}}, \quad (9)$$

where ρ_{nir} and ρ_{swir} are the spectral reflectances of the near infrared and short infrared bands in MODIS imagery, respectively (Xiao, Hollinger, et al., 2004).

3. Data and methods

3.1. Description of study sites

The multi-year flux and meteorology data used in this study were collected from five natural vegetation types with eddy-covariance towers operating in the Chinese Terrestrial Ecosystem Flux Observational Network (ChinaFLUX), including temperate mixed forest (the broad-leaved Korean pine mixed forest in the Changbai Mountains, CBS) and temperate steppe (NM) in North China and alpine shrubland (HBGC), alpine marsh (HBSD) and alpine meadow-steppe (DX) on the Tibetan Plateau. The mean annual precipitation (MAP) is 600–810 mm in CBS, approximately 600 mm in HBGC and HBSD, and 480 mm in DX. The water supply is almost not limited in these vegetation types. NM is located in the semi-arid region with an MAP of 350.9 mm, and water is a dominant factor. A brief description of these vegetation types is presented in Table 1. Detailed information about the climate, vegetation and soil in each vegetation type can be found in the references in Table 1.

Table 3
The coefficients of determination between the maximum photosynthetic capacity (PC_{max}) and environmental factors (MAT: mean annual daily air temperature, $\mathrm{MAT_n}$: mean annual nighttime air temperature, $\mathrm{MAT_d}$: mean annual daytime air temperature, and MAP: mean annual precipitation).

	MAT	$\mathrm{MAT_n}$	$\mathrm{MAT_d}$	MAP
r^2	0.83	0.84	0.74	0.13
p	0.03	0.03	0.06	0.56

3.2. Flux data

Subtracting net ecosystem exchange of CO_2 (NEE; a negative sign denotes carbon entering the ecosystem from the atmosphere, whereas a positive sign denotes carbon release from the ecosystem into the atmosphere) from ecosystem respiration (R_e) gives gross primary production (GPP). NEE was directly measured by the eddy covariance approach. A method presented by Reichstein et al. (2005) was used to estimate R_e. The detailed procedures are presented below.

The original observed half-hourly NEE values were processed by three-dimensional coordinate rotation, WPL correction, storage correction (only for the forest site), and filtering to exclude invalid data (Yu et al., 2006). Missing daytime NEE values (when the solar elevation angle ≥ 0) were calculated with the Michaelis–Menten equation (Michaelis & Menten, 1913). Daytime R_e values were calculated with the Lloyd and Taylor model using the soil temperature at 5 cm depth as the input variable (Lloyd & Taylor, 1994; Reichstein et al., 2005). Valid nighttime NEE (i.e., nighttime respiration when the solar elevation angle < 0) and the soil temperature at 5 cm depth were used to estimate the activation energy parameter (E_0) of the Lloyd and Taylor model every 5 days using a 15-day moving window. The final E_0 for the whole year was calculated as the average of the three E_0 with the smallest standard errors. The reference respiration (R_{ref}) for the Lloyd and Taylor model was estimated every 5 days using a 10-day moving window.

Based on the filled half-hourly daytime NEE data and the calculated daytime R_e, half-hourly GPP values were obtained and then summed to yield daily values. The site-years with more than 10% of the daily GPP values missing were NM in 2006, HBSD in 2007 and DX in 2008. To be consistent with the time scale of the MODIS images, the flux and meteorology data were separately averaged within the same 8-day periods.

3.3. Remote sensing data

EVI, LSWI and MOD11A2 LST products were downloaded from the University of Oklahoma Data Center (http://www.eomf.ou.edu/visualization/manual/). The MOD17 GPP products were downloaded from the Oak Ridge National Laboratory Distributed Active Archive Center (ORNL DAAC. 2012. MODIS subsetted land products, Collection 5. Available on-line [http://daac.ornl.gov/MODIS/modis.html] from ORNL DAAC, Oak Ridge, Tennessee, U.S.A. Accessed 3 29, 2013). All MODIS images were 8-day composites. EVI and LSWI have a spatial resolution of 500 m, and the MOD11A2 LST and the MOD17 GPP products have a

Table 2
The statistics of the PCM parameterization and validation (r^2: coefficient of determination, *SE*: standard error of the simulated GPP, MNB: mean normalized bias, RMSE: root mean square error, and *EF*: modeling efficiency).

Site code	Parameterization						Validation				
	PC_{max} (mol C m^{-2} d^{-1})	r^2	*SE* (mol C m^{-2} d^{-1})	MNB	RMSE (mol C m^{-2} d^{-1})	*EF*	r^2	*SE* (mol C m^{-2} d^{-1})	MNB	RMSE (mol C m^{-2} d^{-1})	*EF*
CBS	2.61	0.92	0.02	−0.24	0.10	0.92	0.93	0.05	−0.24	0.10	0.91
NM	2.06	0.81	0.01	2.76	0.04	0.81	0.83	0.01	2.74	0.04	0.28
NM[a]	2.18	0.83	0.01	2.07	0.04	0.83	0.84	0.01	2.10	0.04	0.77
HBGC	1.75	0.95	0.01	0.48	0.04	0.95	0.95	0.03	0.49	0.04	0.95
HBSD	1.38	0.90	0.01	2.25	0.05	0.90	0.91	0.02	2.26	0.05	0.89
DX	2.00	0.83	0.00	0.26	0.02	0.82	0.85	0.01	0.24	0.03	0.78

[a] The site-year 2005 was excluded from model parameterization and validation due to severe drought. This PC_{max} was chosen as the maximum photosynthetic capacity in NM.

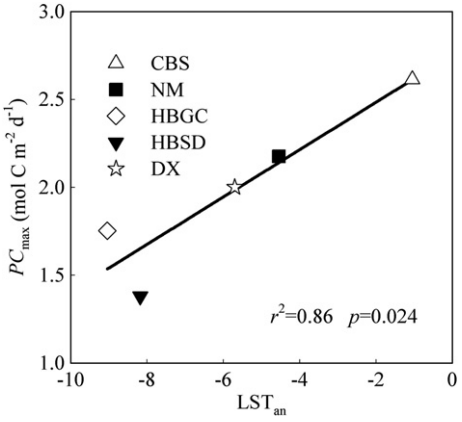

Fig. 2. The relationship between maximum photosynthetic capacity (PC_{max}) and mean annual nighttime LST (LST_{an}). CBS: temperate mixed forest, NM: temperate steppe, HBGC: alpine shrubland, HBSD: alpine marsh, and DX: alpine meadow-steppe.

spatial resolution of 1 km. The pixels in which the flux towers were located were chosen in this study.

3.4. Parameterization and validation

Multi-year eddy CO_2 flux data from five vegetation types in North China (temperate mixed forest and temperate steppe) and the Tibetan Plateau (alpine shrubland, alpine marsh, and alpine meadow-steppe) were used for model parameterization and validation. The site-years with more than 10% of the observed daily GPP values missing, i.e., NM in 2006, HBSD in 2007 and DX in 2008, were excluded from both analyses.

All effective site-year data were used to estimate the model parameter (PC_{max}) for each vegetation type. PC_{max} was taken as the slope of the relationship between the observed GPP and the product of EVI_s and W_s. The model was validated using the method of training/evaluation splitting cross-validation (Migliavacca et al., 2011). The data for each site-year were excluded one at a time, with the remaining site-years as the training data to fit the model parameter, and then to predict the excluded site-year. During the model validation, statistics were calculated and averaged for each vegetation type to assess the performance of the model. The statistics include the coefficient of determination (r^2), standard error (SE), mean normalized bias (MNB), root mean square error (RMSE) and modeling efficiency (EF).

$$r^2 = \left(\frac{\sum_{i=1}^{n} \left(x_i - \bar{x}\right)\left(y_i - \bar{y}\right)}{\sqrt{\sum_{i=1}^{n} \left(x_i - \bar{x}\right)^2 \cdot \sum_{i=1}^{n} \left(y_i - \bar{y}\right)^2}} \right)^2, \tag{10}$$

$$SE = \frac{\sqrt{\sum_{i=1}^{n} (y_i - \bar{y})^2}}{\sqrt{n}}, \tag{11}$$

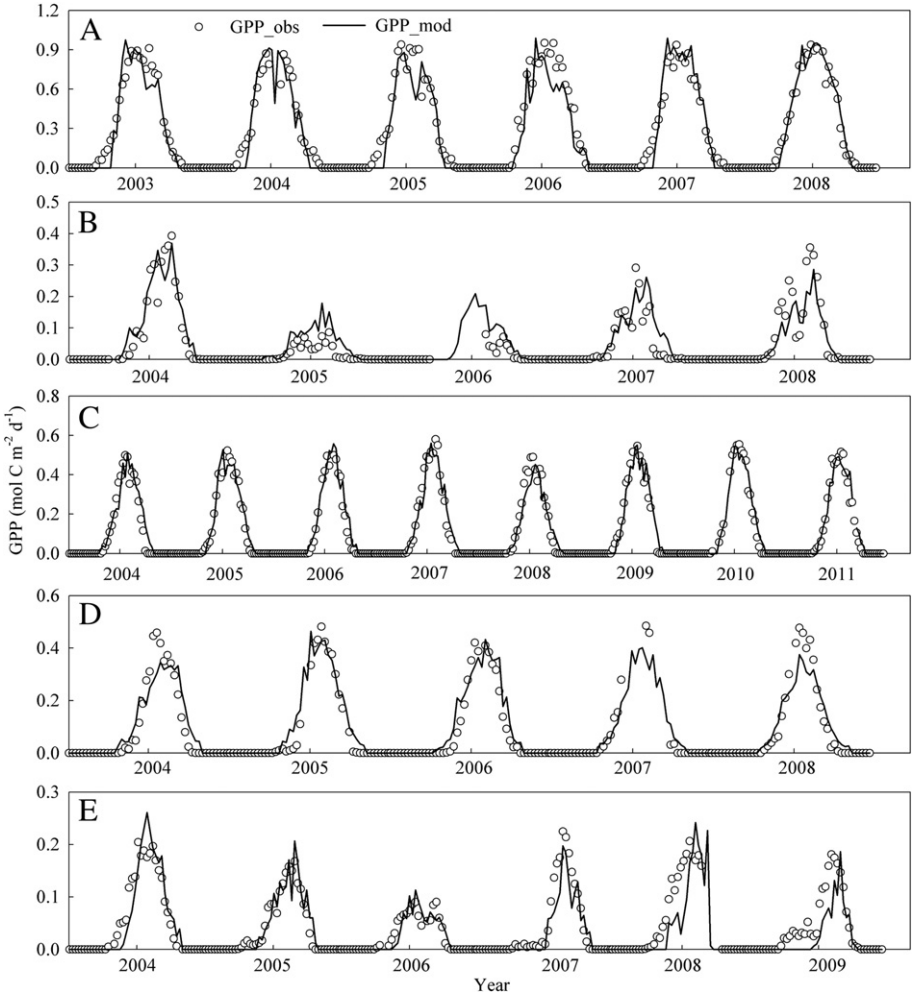

Fig. 3. The seasonal and interannual variation in the observed GPP and simulated GPP, based on an 8-day average. The open dots denote the observed GPP, and the black lines denote the simulated GPP. A: temperate mixed forest (CBS), B: temperate steppe (NM), C: alpine shrubland (HBGC), D: alpine marsh (HBSD), and E: alpine meadow-steppe (DX).

$$\mathrm{MNB} = \frac{1}{n}\sum_{i=1}^{n}\left(\frac{y_i - x_i}{x_i}\right), \tag{12}$$

$$\mathrm{RMSE} = \sqrt{\frac{\sum_{i=1}^{n}(x_i - y_i)^2}{n}}, \tag{13}$$

$$EF = 1 - \frac{\sum_{i=1}^{n}(x_i - y_i)^2}{\sum_{i=1}^{n}\left(x_i - \bar{x}\right)^2}, \tag{14}$$

where the x_i are the observed data, the y_i are the simulated data and x^- and y^- are the averages of the observed and simulated data, respectively. The quantity r^2 represents the fraction of the variation in the observed data that can be explained by the model. MNB and RMSE are used to measure the biases that cause the simulated data to differ from the observations. *EF* represents the consistency of the observed values with the simulated values and is sensitive to the systematic deviation. *EF* can range from $-\infty$ to 1. An efficiency of 1 ($EF = 1$) corresponds to a perfect match between the simulated data and the observed data. An efficiency of 0 ($EF = 0$) indicates that the model estimates are as accurate as the mean of the observed data. An efficiency less than 0 ($EF < 0$) indicates that the observed mean is a better predictor than the model.

4. Results

4.1. PC_{max}

The observed 8-day average GPP was linearly related to $EVI_s \times W_s$ in each vegetation type (Fig. 1), and the slope of this linear relationship was identified as the maximum photosynthetic capacity (PC_{max}, mol C m^{-2} d^{-1}). The model parameterization showed that PC_{max} was lowest in HBSD, highest in CBS and similar in NM and DX (Table 2). Due to a severe drought in NM in 2005 (precipitation was less than 200 mm), this site-year was removed from the model parameterization.

A regression analysis of PC_{max} as a function of the ground-observed mean annual daily air temperature (MAT), nighttime air temperature (MAT_n, when the solar elevation angle < 0), daytime air temperature (MAT_d, when the solar elevation angle ≥ 0) or precipitation (MAP) during the study periods indicated that PC_{max} had significant relationships with MAT and MAT_n (Table 3). Because of the strong relationship between the MAT_n and the mean annual nighttime Land Surface Temperature (LST_{an}) from MODIS LST products, LST_{an} can explain

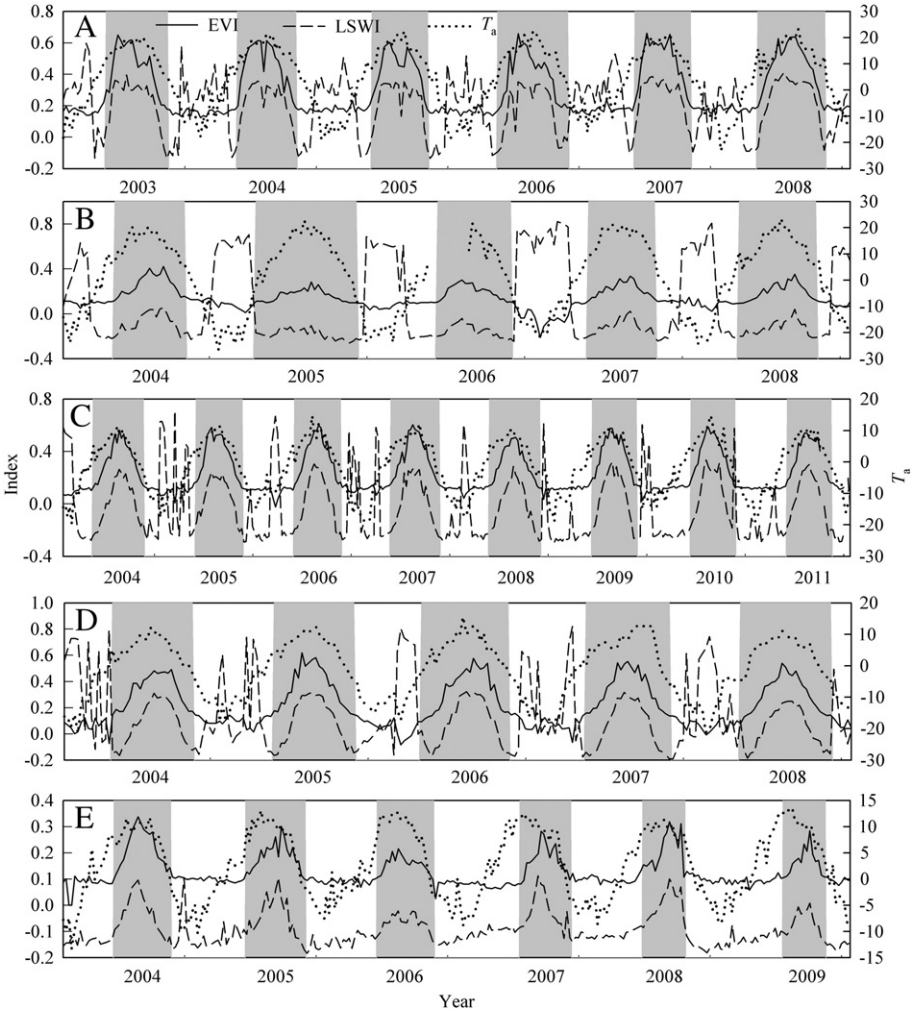

Fig. 4. The seasonal and interannual variation in EVI, LSWI and air temperature (T_a), based on an 8-day average. The gray shadows indicate the growing season that was identified from the EVI time series (Zhang et al., 2003). A: temperate mixed forest (CBS), B: temperate steppe (NM), C: alpine shrubland (HBGC), D: alpine marsh (HBSD), and E: alpine meadow-steppe (DX).

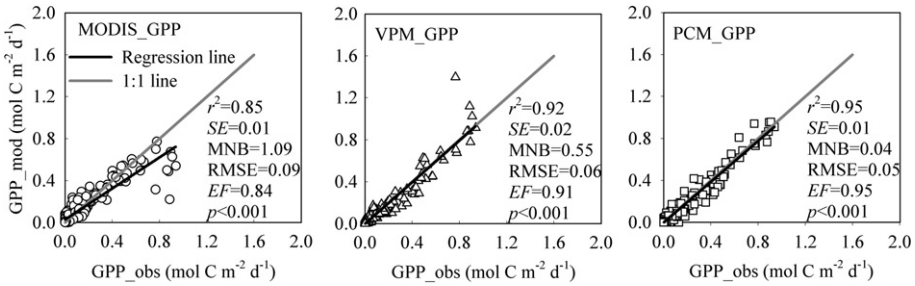

Fig. 5. Comparisons of the observed GPP with the predicted GPP from the PCM, the MODIS GPP products and the VPM, based on an 8-day average. The plots are derived from the last year of the time series for each vegetation type (Table 1). r^2: coefficient of determination, *SE*: standard error of the simulated GPP (mol C m^{-2} d^{-1}), MNB: mean normalized bias, RMSE: root mean square error (mol C m^{-2} d^{-1}), and *EF*: modeling efficiency. In the VPM, the phenology factor was set to 1, and the minimum, maximum and optimum temperatures for photosynthetic activities were separately assumed to be 0, 35 and 20 °C for all five vegetation types (for details see Wu et al. (2009) for CBS, Li et al. (2007) for HBGC and HBSD, and Li et al. (2007) and Liu, Chen, and Han (2012) for NM and DX). PAR was calculated from shortwave radiation (*SW*) using the equation of $SW \approx 0.505 \times \mathrm{PAR}$ (Unit: PAR, mol m^{-2} s^{-1}; *SW*, W m^{-2}; Mahadevan et al., 2008).

approximately 86% of the variation in PC_{max} (Table 2). Thus, the following linear equation in LST_{an} can be used to estimate the spatial variation in PC_{max} (Fig. 2):

$$PC_{max} = 0.1346 \times LST_{an} + 2.7522. \quad (15)$$

4.2. Seasonal and inter-seasonal dynamics of the PCM-estimated GPP

Using the parameterized PC_{max} in Table 2, the PCM was executed to estimate GPP for all site-years for each vegetation type (Fig. 3). In most cases, the beginning and ending dates of the simulated GPP agreed well with those of the observed GPP, and the simulated maximal GPP was also in good agreement with the observed maximal GPP. The PCM-simulated GPP and the flux-observed GPP displayed most consistent seasonal and inter-seasonal variations in HBGC, followed by CBS and HBSD (Table. 2, Fig. 3A, C and D). However, NM and DX showed several obvious gaps. When a severe drought occurred, i.e., during 2005 in NM (Fig. 4B), a large discrepancy resulted between the simulated GPP and the observed GPP (Fig. 3B). When the vegetation was very sparse, e.g., at the early stage of the 2009 growing season in DX (Fig. 4E), the beginning date of the simulated GPP obviously lagged behind that of the observed GPP (Fig. 3E). These results indicated that the PCM performs well in GPP estimation except under conditions of serious drought and very sparse vegetation.

4.3. Comparison of the predictive accuracy of the PCM with the MODIS GPP products and the VPM

Across the studied vegetation types, the statistics from the model validation were similar to the values from the model parameterization (Table 2). The model validation showed that the PCM can predict 84–95% of the variation in the observed GPP.

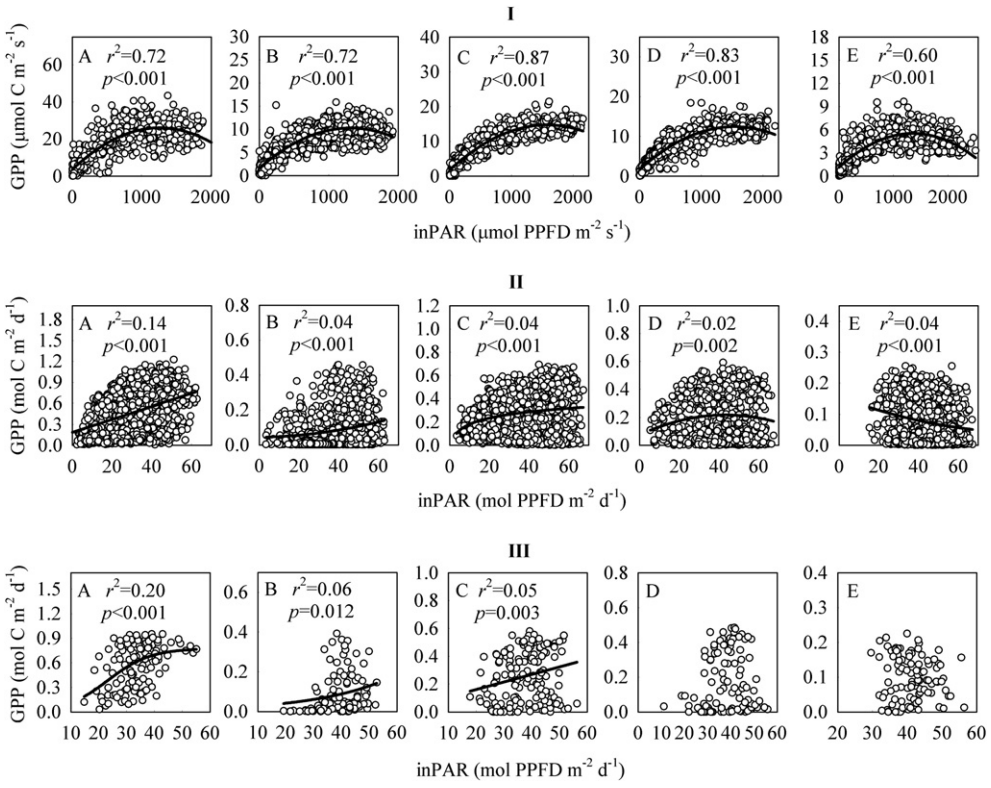

Fig. 6. The observed GPP plotted against (I) half-hourly incident PAR (inPAR) during the peak growing season of the first year in Table 1 (taken as an example), (II) daily inPAR during the growing season for the study periods and (III) 8-day average inPAR during the growing season for the study periods. The inPAR was calculated from the shortwave radiation (*SW*) using the equation of $SW \approx 0.505 \times \mathrm{PAR}$ (Unit: PAR, mol m^{-2} s^{-1}; *SW*, W m^{-2}; Mahadevan et al., 2008). A: temperate mixed forest (CBS), B: temperate steppe (NM), C: alpine shrubland (HBGC), D: alpine marsh (HBSD), and E: alpine meadow-steppe (DX).

To further assess the performance of the PCM in GPP prediction, one-year data (the last year of the time series for each vegetation type) in Table 1 were chosen to compare the predictive accuracy of the PCM with that of the MODIS GPP products and the VPM. The MODIS GPP products are the principal source of GPP at regional and global scales (Running et al., 2004; http://daac.ornl.gov/MODIS/modis.html), and the VPM is a MODIS-based LUE model and has been validated in four of our studied vegetation types (Li et al., 2007; Wu et al., 2008, 2009; Zhang et al., 2009). Plots of the predicted GPP against the observed GPP for these three models are presented in Fig. 5. According to the values of the statistics, the predictive accuracy of the PCM was higher than that of the MODIS GPP products and comparable with the VPM. The regression line of the observed GPP vs. either the PCM-predicted GPP or VPM-predicted GPP was very close to the 1:1 line. The MODIS GPP products appeared to overestimate the lower values of the observed GPP and to underestimate the higher values of the observed GPP. Similar biases of the MODIS GPP products have also been reported in other studies (e.g., He et al., 2013; Turner et al., 2006; Zhang, Yu, Jiang, & Tang, 2008).

5. Discussion

5.1. Impact of photosynthetically active radiation on photosynthesis

As the essential energy source, incident PAR (inPAR) is an important input variable in light use efficiency models (e.g., Monteith, 1972; Potter et al., 1993; Prince & Goward, 1995; Xiao, Hollinger, et al., 2004). In our study region during the peak growing season, when inPAR has the most direct influence on photosynthesis (Fig. 6I), there are generally three types of relationships between GPP and inPAR over short time periods (minutes to hours): positive (light limited), irrelevant (light saturation) and negative (light exceeds what plants need). If the half-hourly GPP and inPAR were summed to obtain daily values (Fig. 6II) or further averaged to 8-day values over the growing season in the study periods (Fig. 6III), GPP had little or no relationship with inPAR. Although the GPP-inPAR response was analyzed separately for each site-year, r^2 was nearly as low as in the all site-years in each vegetation type (data not shown). These results indicated that inPAR only slightly constrains photosynthesis on an 8-day time scale in our studied vegetation types.

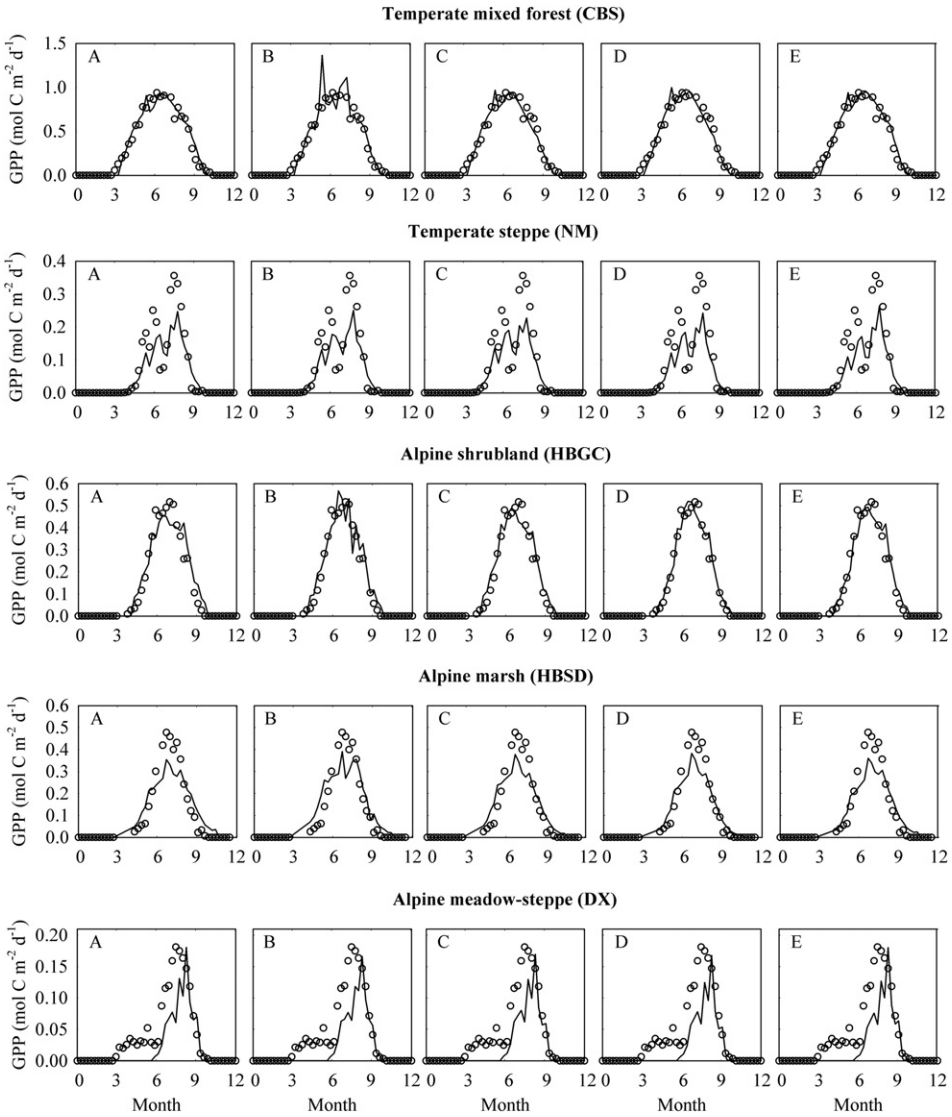

Fig. 7. Comparison between the observed GPP and the predicted GPP, based on an 8-day average. The predicted GPP values were calculated from five formulas for the GPP model, with the following driving variables: A, EVI_s alone; B, $EVI_s \times$ incident PAR ($EVI_s \times$ inPAR); C, $EVI_s \times$ potential PAR ($EVI_s \times$ pPAR); D, $EVI_s \times$ potential PAR $\times W_s$ ($EVI_s \times$ pPAR $\times W_s$); and E, $EVI_s \times W_s$ (i.e., the PCM). The data are derived from the last year of the time series for each vegetation type (Table 1). W_s: moisture index. The open dots denote the observed GPP, and the black lines denote the predicted GPP.

Table 4
The statistics of the predicted GPP from five formulas for the GPP model, which were separately driven by EVI_s alone, EVI_s × incident PAR (EVI_s × inPAR), EVI_s × potential PAR (EVI_s × pPAR), EVI_s × potential PAR × W_s (EVI_s × pPAR × W_s) and EVI_s × W_s (i.e. the PCM). The data are derived from the last year of the time series for each vegetation type (Table 1). W_s: moisture index. r^2: coefficient of determination, *SE*: standard error of the simulated GPP, MNB: mean normalized bias, RMSE: root mean square error, and *EF*: modeling efficiency. CBS: temperate mixed forest, NM: temperate steppe, HBGC: alpine shrubland, HBSD: alpine marsh, and DX: alpine meadow-steppe.

Site code	Formula	r^2	*SE* (mol C m^{-2} d^{-1})	MNB	RMSE (mol C m^{-2} d^{-1})	*EF*
CBS	EVI_s	0.97	0.05	−0.04	0.06	0.97
	EVI_s × inPAR	0.92	0.06	−0.09	0.11	0.90
	EVI_s × pPAR	0.97	0.05	−0.14	0.06	0.97
	EVI_s × pPAR × W_s	0.97	0.05	−0.17	0.06	0.97
	EVI_s × W_s	0.97	0.05	−0.09	0.06	0.97
NM	EVI_s	0.86	0.01	0.69	0.05	0.78
	EVI_s × inPAR	0.85	0.01	0.51	0.05	0.78
	EVI_s × pPAR	0.85	0.01	0.41	0.05	0.77
	EVI_s × PAR × W_s	0.85	0.01	0.23	0.05	0.76
	EVI_s × W_s	0.86	0.01	0.45	0.05	0.77
HBGC	EVI_s	0.93	0.03	0.23	0.05	0.93
	EVI_s × inPAR	0.95	0.03	0.18	0.04	0.95
	EVI_s × $pPAR_p$	0.96	0.03	0.17	0.04	0.95
	EVI_s × pPAR × W_s	0.97	0.03	0.02	0.03	0.97
	EVI_s × W_s	0.96	0.03	0.06	0.04	0.96
HBSD	EVI_s	0.88	0.02	0.89	0.06	0.85
	EVI_s × inPAR	0.86	0.02	0.91	0.06	0.85
	EVI_s × pPAR	0.91	0.02	0.66	0.06	0.87
	EVI_s × pPAR × W_s	0.94	0.02	0.40	0.05	0.90
	EVI_s × W_s	0.92	0.02	0.58	0.05	0.88
DX	EVI_s	0.75	0.01	−0.58	0.03	0.64
	EVI_s × inPAR	0.79	0.01	−0.58	0.03	0.66
	EVI_s × pPAR	0.79	0.01	−0.61	0.03	0.65
	EVI_s × PAR × W_s	0.78	0.01	−0.64	0.03	0.62
	EVI_s × W_s	0.74	0.01	−0.61	0.03	0.62

The temporal variability of inPAR during growing season reflects two types of variation: low-frequency variation due to seasonal change in the hours of sunshine (i.e., day length) and high-frequency variation caused by constantly changing atmospheric conditions (Gitelson et al., 2012; Sakamoto et al., 2011). It has been showed that the high-frequency variation in inPAR can introduce large uncertainties into crop GPP estimation, whereas potential PAR (pPAR), which represents only the low-frequency variation in inPAR, performs better than inPAR (Gitelson et al., 2012; Peng et al., 2013). Unlike the PCM, which uses EVI to represent the photosynthetic capacity, many studies have employed EVI to indicate the fraction of PAR absorbed by the photosynthetically active parts of the plant canopy (Kalfas et al., 2011; Li et al., 2007; Wu et al., 2008; Xiao, Hollinger, et al., 2004; Xiao, Zhang, et al., 2004; Xiao et al., 2005; Yan et al., 2009). To identify the weight of each item in GPP estimation, five formulas for the GPP model, driven separately by EVI_s alone (model A), EVI_s × inPAR (model B), EVI_s × pPAR (model C), EVI_s × pPAR × W_s (model D) and EVI_s × W_s (model E, i.e., PCM), were built to predict GPP (the last year of the time series for each vegetation type, Table 1), and the outputs were compared with the observed GPP (Fig. 7, Table. 4). The results showed that model B was not significantly improved over model A (Fig. 7A and B, Table 4), whereas the model with pPAR as an input variable performed better in GPP prediction than that with inPAR (Fig. 7B, C and D, Table 4). These findings are consistent with the studies in crops (Gitelson et al., 2012; Peng et al., 2013). According to the various statistics used to assess the performance of the models (Table 4), the predictive accuracy of model E is comparable with that of the potential PAR-based models (Fig. 7C, D and E). This is probably because the potential PAR largely determines the environmental temperature and thus drives the dynamic changes in canopy chlorophyll content in our study region. Both the potential PAR and the total content of canopy chlorophyll show similar seasonal variation and can be effectively represented by EVI.

5.2. Impacts of temperature and moisture on photosynthesis

A number of LUE models incorporate moisture and/or temperature as important environmental controls in plant photosynthesis (Prince & Goward, 1995; Running et al., 2004; Xiao, Hollinger, et al., 2004). Because GPP generally has a sigmoidal relationship with temperature (Fig. 8), the temperature equation (TEMP) developed for the Terrestrial Ecosystem Model (TEM) has proven effective in expressing the effect of temperature on photosynthesis (Raich et al., 1991). In the TEMP, minimum, maximum and optimal temperatures for photosynthetic activities are three necessary input parameters and are, therefore, important in GPP estimation. However, these three temperatures are derived from either ground observations or the literature, both of which limit the spatial application of TEMP-based GPP models. Furthermore, temperature primarily controls photosynthesis at the beginning and end of the growing season (Chen et al., 2005; Linkosalo, 2000; Yuan et al., 2007), which can be represented effectively by the EVI time series (Zhang et al., 2003). Thus, the PCM does not include temperature as a constraint. However, whether the PCM is effective in GPP estimation when the temperature is extremely high or low has not been examined because these conditions did not occur during the study period (Fig. 4).

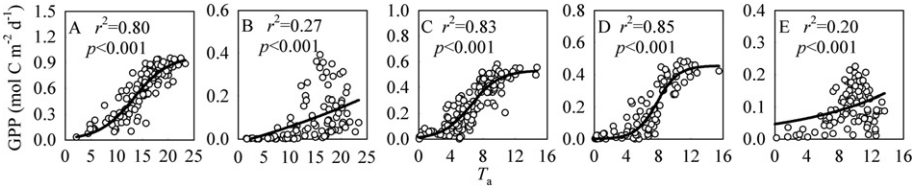

Fig. 8. Plots of the observed GPP against air temperature (T_a), based on an 8-day average during the growing season. A: temperate mixed forest (CBS), B: temperate steppe (NM), C: alpine shrubland (HBGC), D: alpine marsh (HBSD), and E: alpine meadow-steppe (DX).

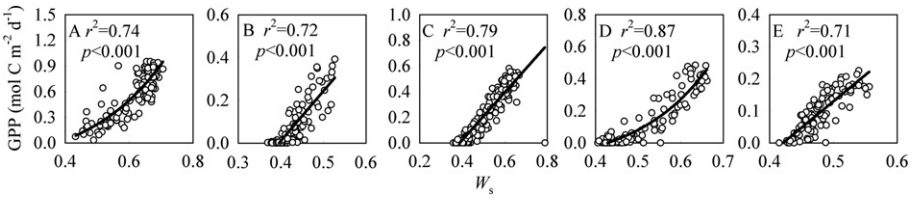

Fig. 9. Plots of the observed GPP against moisture index (W_s), based on an 8-day average during the growing season. A: temperate mixed forest (CBS), B: temperate steppe (NM), C: alpine shrubland (HBGC), D: alpine marsh (HBSD), and E: alpine meadow-steppe (DX).

Although the observed GPP responds almost linearly to the moisture index during the growing season in each vegetation type (Fig. 9), the PCM does not perform well under conditions of serious drought (NM in 2005, Fig. 3B).

5.3. Application of the PCM at regional scale

The PCM can potentially be used in regional GPP estimation. The PCM follows Monteith's (1972, 1977) logic and is entirely driven by the MODIS imagery. This approach avoids the introduction of substantial simulation errors into regional estimation due to the coarse spatial resolution of ground observations (Rahman et al., 2005; Sims et al., 2008; Wu, Niu, & Gao, 2010; Yang et al., 2007). The model parameter (PC_{max}) has a clear ecological meaning and is linearly correlated with the mean annual nighttime LST retrieved from MODIS imagery. Using this linear equation, Eq. (15), to replace the PC_{max} in the PCM, the PCM-simulated GPP can explain 93% of the variation in the flux-observed GPP across all five vegetation types (Fig. 10). Furthermore, with the development of remote sensing techniques and algorithms related to canopy chlorophyll content and moisture conditions, the PCM is promising to provide more accurate estimates of GPP.

6. Conclusions

This study developed a MODIS-based Photosynthetic Capacity Model (PCM) for simulating gross primary production (GPP) of terrestrial ecosystems in North China and the Tibetan Plateau. The PCM follows Monteith's logic and is driven solely by the Enhanced Vegetation Index (EVI) and the Land Surface Water Index (LSWI) from MODIS imagery. The predictive accuracy of the PCM was higher than that of the MOD17 products and comparable with the VPM and the potential PAR-based GPP model. The model parameter (PC_{max}) that represents the maximum photosynthetic capacity had a close linear relationship with the MODIS-derived mean annual nighttime Land Surface Temperature (LST_{an}). This relationship provides a possible approach to the use of the PCM to estimate GPP at a regional scale. However, the performance of the PCM in other vegetation types or regions still needs further study.

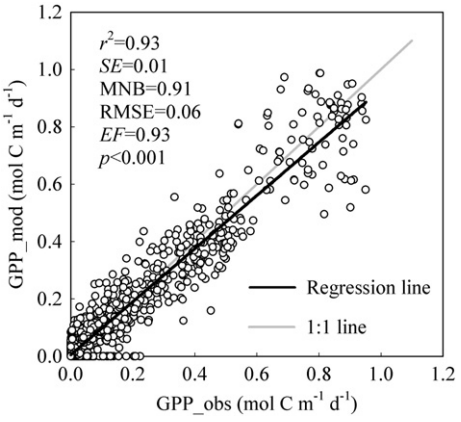

Fig. 10. Comparison between the flux-observed GPP and the PCM-simulated GPP, based on an 8-day average. The PC_{max} of the PCM was calculated from Eq. (15). Multi-year data from all five vegetation types are plotted in the figure. r^2: coefficient of determination, *SE*: standard error of the simulated GPP (mol C m^{-2} d^{-1}), MNB: mean normalized bias, RMSE: root mean square error (mol C m^{-2} d^{-1}), and *EF*: modeling efficiency.

Acknowledgments

This research was funded by the National Key Research and Development Program (Grant No. 2010CB833504), the CAS Strategic Priority Research Program (Grant No. XDA05050600), and the National Natural Science Foundation of China (Grant No. 31290220). We sincerely thank the anonymous reviewers for their constructive comments and suggestions.

References

Alton, P. B., North, P. R., & Los, S. O. (2007). The impact of diffuse sunlight on canopy light-use efficiency, gross photosynthetic product and net ecosystem exchange in three forest biomes. *Global Change Biology*, *13*, 776–787.

Beer, C., Reichstein, M., Tomelleri, E., Ciais, P., Jung, M., Carvalhais, N., et al. (2010). Terrestrial gross carbon dioxide uptake: Global distribution and covariation with climate. *Science*, *329*, 834–838.

Chapin, F. S., III, Matson, P. A., & Vitousek, P.M. (2011). *Principles of terrestrial ecosystem ecology* (2th ed.). New York: Springer Science + Business Media.

Chen, X., Hu, B., & Yu, R. (2005). Spatial and temporal variation of phenological growing season and climate change impacts in temperate eastern China. *Global Change Biology*, *11*, 1118–1130.

Ehleringer, J. R., Björkman, O., & Mooney, H. A. (1976). Leaf pubescence: Effects on absorptance and photosynthesis in a desert shrub. *Science*, *192*, 376–377.

Fu, Y., Zheng, Z., Yu, G., Hu, Z., Sun, X., Shi, P., et al. (2009). Environmental influences on carbon dioxide fluxes over three grassland ecosystems in China. *Biogeosciences*, *6*, 2879–2893.

Garbulsky, M. F., Peñuelas, J., Papale, D., Ardö, J., Goulden, M. L., Kiely, G., et al. (2010). Patterns and controls of the variability of radiation use efficiency and primary productivity across terrestrial ecosystems. *Global Ecology and Biogeography*, *19*, 253–267.

Gitelson, A. A., Peng, Y., Masek, J. G., Rundquist, D. C., Verma, S., Suyker, A., et al. (2012). Remote estimation of crop gross primary production with Landsat data. *Remote Sensing of Environment*, *121*, 404–414.

Gitelson, A. A., Viña, A., Ciganda, V., Rundquist, D. C., & Arkebauer, T. J. (2005). Remote estimation of canopy chlorophyll content in crops. *Geophysical Research Letters*, *32*, L08403. http://dx.doi.org/10.1029/2005GL022688.

Gitelson, A. A., Viña, A., Verma, S. B., Rundquist, D. C., Arkebauer, T. J., Keydan, G., et al. (2006). Relationship between gross primary production and chlorophyll content in crops: Implications for the synoptic monitoring of vegetation productivity. *Journal of Geophysical Research-Atmospheres*, *111*, D08S11. http://dx.doi.org/10.1029/2005JD006017.

He, M., Zhou, Y., Ju, W., Chen, J., Zhang, L., Wang, S., et al. (2013). Evaluation and improvement of MODIS gross primary productivity in typical forest ecosystems of East Asia based on eddy covariance measurements. *Journal of Forest Research*, *18*, 31–40.

Huang, N., Niu, Z., Zhan, Y., Xu, S., Tappert, M. C., Wu, C., et al. (2012). Relationships between soil respiration and photosynthesis-related spectral vegetation indices in two cropland ecosystems. *Agricultural and Forest Meteorology*, *160*, 80–89.

Huete, A., Didan, K., Miura, T., Rodriguez, E. P., Gao, X., & Ferreira, L. G. (2002). Overview of the radiometric and biophysical performance of the MODIS vegetation indices. *Remote Sensing of Environment*, *83*, 195–213.

Hunt, E. R., Jr., Doraiswamy, P. C., McMurtrey, J. E., Daughtry, C. S. T., Perry, E. M., & Akhmedov, B. (2013). A visible band index for remote sensing leaf chlorophyll content at the canopy scale. *International Journal of Applied Earth Observation and Geoinformation*, *21*, 103–112.

Ibrom, A., Oltchev, A., June, T., Kreilein, H., Rakkibu, G., Ross, T., et al. (2008). Variation in photosynthetic light-use efficiency in a mountainous tropical rain forest in Indonesia. *Tree Physiology*, *28*, 499–508.

Ide, R., Nakaji, T., & Oguma, H. (2010). Assessment of canopy photosynthetic capacity and estimation of GPP by using spectral vegetation indices and the light-response function in a larch forest. *Agricultural and Forest Meteorology*, *150*, 389–398.

Kalfas, J. L., Xiao, X., Vanegas, D. X., Verma, S. B., & Suyker, A. E. (2011). Modeling gross primary production of irrigated and rain-fed maize using MODIS imagery and CO_2 flux tower data. *Agricultural and Forest Meteorology*, *151*, 1514–1528.
Koller, D. (2000). Plants in search of sunlight. *Advances in Botanical Research*, *33*, 35–131.
Lagergren, F., Eklundh, L., Grelle, A., Lundblad, M., Mölder, M., Lankreijer, H., et al. (2005). Net primary production and light use efficiency in a mixed coniferous forest in Sweden. *Plant, Cell and Environment*, *28*, 412–423.
Li, Z., Yu, G., Xiao, X., Li, Y., Zhao, X., Ren, C., et al. (2007). Modeling gross primary production of alpine ecosystems in the Tibetan Plateau using MODIS images and climate data. *Remote Sensing of Environment*, *107*, 510–519.
Linkosalo, T. (2000). Mutual regularity of spring phenology of some boreal tree species: Predicting with other species and phenological models. *Canadian Journal of Forest Research*, *30*, 667–673.
Liu, J., Chen, S., & Han, X. (2012). Modeling gross primary production of two steppes in Northern China using MODIS time series and climate data. *Procedia Environmental Sciences*, *13*, 742–754.
Lloyd, J., & Taylor, J. A. (1994). On the temperature dependence of soil respiration. *Functional Ecology*, *8*, 315–323.
Mahadevan, P., Wofsy, S.C., Matross, D.M., Xiao, X., Dunn, A. L., Lin, J. C., et al. (2008). A satellite-based biosphere parameterization for net ecosystem CO_2 exchange: Vegetation Photosynthesis and Respiration Model (VPRM). *Global Biogeochemical Cycles*, *22*, GB2005. http://dx.doi.org/10.1029/2006GB002735.
Medina, E., & Lieth, H. (1964). Die Beziehungen zwischen Chlorophyllgehalt, assimilierender Flaeche und Trockensubstanzproduktion in einigen Pflanzengemeinschaften [The relationships between chlorophyll content, assimilating area and dry matter production in some plant communities]. *Beitraege zur Biologie der Pflanzen*, *40*, 451–494.
Michaelis, L., & Menten, M. L. (1913). The kinetics of the inversion effect. *Biochemische Zeitschrift*, *49*, 333–369.
Migliavacca, M., Reichstein, M., Richardson, A.D., Colombo, R., Sutton, M.A., Lasslop, G., et al. (2011). Semiempirical modeling of abiotic and biotic factors controlling ecosystem respiration across eddy covariance sites. *Global Change Biology*, *17*, 390–409.
Monteith, J. L. (1972). Solar radiation and productivity in tropical ecosystems. *Journal of Applied Ecology*, *9*, 747–766.
Monteith, J. L. (1977). Climate and the efficiency of crop production in Britain. *Philosophical Transactions of the Royal Society of London Series B-Biological Sciences*, *281*, 277–294.
Muraoka, H., & Koizumi, H. (2005). Photosynthetic and structural characteristics of canopy and shrub trees in a cool-temperate deciduous broadleaved forest: Implication to the ecosystem carbon gain. *Agricultural and Forest Meteorology*, *134*, 39–59.
Muraoka, H., Noda, H. M., Nagai, S., Motohka, T., Saitoh, T. M., Nasahara, K. N., et al. (2013). Spectral vegetation indices as the indicator of canopy photosynthetic productivity in a deciduous broadleaf forest. *Journal of Plant Ecology*, *6*, 393–407.
Nagai, S., Saigusa, N., Muraoka, H., & Nasahara, K. N. (2010). What makes the satellite-based EVI–GPP relationship unclear in a deciduous broad-leaved forest? *Ecological Research*, *25*, 359–365.
Peng, Y., Gitelson, A. A., Keydan, G., Rundquist, D. C., & Moses, W. (2011). Remote estimation of gross primary production in maize and support for a new paradigm based on total crop chlorophyll content. *Remote Sensing of Environment*, *115*, 978–989.
Peng, Y., Gitelson, A. A., & Sakamoto, T. (2013). Remote estimation of gross primary productivity in crops using MODIS 250 m data. *Remote Sensing of Environment*, *128*, 186–196.
Potter, C. S., Randerson, J. T., Field, C. B., Matson, P. A., Vitousek, P.M., Mooney, H. A., et al. (1993). Terrestrial ecosystem production: A process model based on global satellite and surface data. *Global Biogeochemical Cycles*, *7*, 811–841.
Prince, S. D., & Goward, S. N. (1995). Global primary production: A remote sensing approach. *Journal of Biogeography*, *22*, 815–835.
Propastin, P., Ibrom, A., Knohl, A., & Erasmi, S. (2012). Effects of canopy photosynthesis saturation on the estimation of gross primary productivity from MODIS data in a tropical forest. *Remote Sensing of Environment*, *121*, 252–260.
Rahman, A. F., Sims, D. A., Cordova, V. D., & El-Masri, B. Z. (2005). Potential of MODIS EVI and surface temperature for directly estimating per-pixel ecosystem C fluxes. *Geophysical Research Letters*, *32*, L19404. http://dx.doi.org/10.1029/2005GL024127.
Raich, J., Rastetter, E., Melillo, J., Kicklighter, D., Steudler, P., Peterson, B., et al. (1991). Potential net primary productivity in South America: Application of a global model. *Ecological Applications*, *1*, 399–429.
Reichstein, M., Falge, E., Baldocchi, D., Papale, D., Aubinet, M., Berbigier, P., et al. (2005). On the separation of net ecosystem exchange into assimilation and ecosystem respiration: Review and improved algorithm. *Global Change Biology*, *11*, 1424–1439.
Running, S. W., Nemani, R. R., Heinsch, F. A., Zhao, M., Reeves, M., & Hashimoto, H. (2004). A continuous satellite-derived measure of global terrestrial primary production. *Bioscience*, *54*, 547–560.
Sakamoto, T., Gitelson, A. A., Wardlow, B.D., Verma, S. B., & Suyker, A. E. (2011). Estimating daily gross primary production of maize based only on MODIS WDRVI and shortwave radiation data. *Remote Sensing of Environment*, *115*, 3091–3101.
Schlemmer, M., Gitelson, A., Schepers, J., Ferguson, R., Peng, Y., Shanahan, J., et al. (2013). Remote estimation of nitrogen and chlorophyll contents in maize at leaf and canopy levels. *International Journal of Applied Earth Observation and Geoinformation*, *25*, 47–54.
Scott, R. L., Hamerlynck, E. P., Jenerette, G. D., Moran, M. S., & Barron-Gafford, G. A. (2010). Carbon dioxide exchange in a semidesert grassland through drought-induced vegetation change. *Journal of Geophysical Research-Biogeosciences*, *115*, G03026. http://dx.doi.org/10.1029/2010JG001348.
Sims, D. A., Rahman, A. F., Cordova, V. D., Baldocchi, D.D., Flanagan, L. B., & Goldstein, A. H. (2005). Midday values of gross CO_2 flux and light use efficiency during satellite overpasses can be used to directly estimate eight-day mean flux. *Agricultural and Forest Meteorology*, *131*, 1–12.
Sims, D. A., Rahman, A. F., Cordova, V. D., El-Masri, B. Z., Baldocchi, D.D., Bolstad, P. V., et al. (2008). A new model of gross primary productivity for North American ecosystems based solely on the enhanced vegetation index and land surface temperature from MODIS. *Remote Sensing of Environment*, *112*, 1633–1646.
Sims, D. A., Rahman, A. F., Cordova, V. D., El-Masri, B. Z., Baldocchi, D.D., Flanagan, L. B., et al. (2006). On the use of MODIS EVI to assess gross primary productivity of North American ecosystems. *Journal of Geophysical Research-Biogeosciences*, *111*, G04015. http://dx.doi.org/10.1029/2006JG000162.
Sjöström, M., Ardö, J., Arneth, A., Boulain, N., Cappelaere, B., Eklundh, L., et al. (2011). Exploring the potential of MODIS EVI for modeling gross primary production across African ecosystems. *Remote Sensing of Environment*, *115*, 1081–1089.
Taiz, L., & Zeiger, E. (2002). *Plant physiology* (3th ed.). Sunderland: Sinauer Associates.
Turner, D. P., Ritts, W. D., Cohen, W. B., Gower, S. T., Running, S. W., Zhao, M., et al. (2006). Evaluation of MODIS NPP and GPP products across multiple biomes. *Remote Sensing of Environment*, *102*, 282–292.
Turner, D. P., Urbanski, S., Bremer, D., Wofsy, S.C., Meyers, T., Gower, S. T., et al. (2003). A cross-biome comparison of daily light use efficiency for gross primary production. *Global Change Biology*, *9*, 383–395.
Whittaker, R. H., & Marks, P. L. (1975). Methods of assessing terrestrial productivity. In H. Lieth & R.H. Whittaker (Eds.), *Primary productivity of the biosphere. Ecological Studies*, *14*. (pp. 55–118). New York: Springer-erlag.
Wu, C., Chen, J., & Huang, N. (2011). Predicting gross primary production from the enhanced vegetation index and photosynthetically active radiation: Evaluation and calibration. *Remote Sensing of Environment*, *115*, 3424–3435.
Wu, C., Munger, J. W., Niu, Z., & Kuang, D. (2010). Comparison of multiple models for estimating gross primary production using MODIS and eddy covariance data in Harvard Forest. *Remote Sensing of Environment*, *114*, 2925–2939.
Wu, C., Niu, Z., & Gao, S. (2010). Gross primary production estimation from MODIS data with vegetation index and photosynthetically active radiation in maize. *Journal of Geophysical Research-Atmospheres*, *115*, D12127. http://dx.doi.org/10.1029/2009JD013023.
Wu, W., Wang, S., Xiao, X., Yu, G., Fu, Y., & Hao, Y. (2008). Modeling gross primary production of a temperate grassland ecosystem in Inner Mongolia, China, using MODIS imagery and climate data. *Science in China Series D: Earth Sciences*, *51*, 1501–1512.
Wu, J., Xiao, X., Guan, D., Shi, T., Jin, C., & Han, S. (2009). Estimation of the gross primary production of an old-growth temperate mixed forest using eddy covariance and remote sensing. *International Journal of Remote Sensing*, *30*, 463–479.
Xiao, X., Hollinger, D., Aber, J., Goltz, M., Davidson, E. A., Zhang, Q., et al. (2004). Satellite-based modeling of gross primary production in an evergreen needleleaf forest. *Remote Sensing of Environment*, *89*, 519–534.
Xiao, X., Zhang, Q., Braswell, B., Urbanski, S., Boles, S., Wofsy, S., et al. (2004). Modeling gross primary production of temperate deciduous broadleaf forest using satellite images and climate data. *Remote Sensing of Environment*, *91*, 256–270.
Xiao, X., Zhang, Q., Saleska, S., Hutyra, L., De Camargo, P., Wofsy, S., et al. (2005). Satellite-based modeling of gross primary production in a seasonally moist tropical evergreen forest. *Remote Sensing of Environment*, *94*, 105–122.
Yan, H., Fu, Y., Xiao, X., Huang, H. Q., He, H., & Ediger, L. (2009). Modeling gross primary productivity for winter wheat–maize double cropping system using MODIS time series and CO_2 eddy flux tower data. *Agriculture, Ecosystems & Environment*, *129*, 391–400.
Yang, F., Ichii, K., White, M.A., Hashimoto, H., Michaelis, A.R., Votava, P., et al. (2007). Developing a continental-scale measure of gross primary production by combining MODIS and AmeriFlux data through Support Vector Machine approach. *Remote Sensing of Environment*, *110*, 109–122.
Yang, Y., Shang, S., Guan, H., & Jiang, L. (2013). A novel algorithm to assess gross primary production for terrestrial ecosystems from MODIS imagery. *Journal of Geophysical Research-Biogeosciences*, *118*. http://dx.doi.org/10.1002/jgrg.20056.
Yu, G., Wen, X., Sun, X., Tanner, B.D., Lee, X., & Chen, J. (2006). Overview of ChinaFLUX and evaluation of its eddy covariance measurement. *Agricultural and Forest Meteorology*, *137*, 125–137.
Yu, G., Zhu, X., Fu, Y., He, H., Wang, Q., Wen, X., et al. (2013). Spatial patterns and climate drivers of carbon fluxes in terrestrial ecosystems of China. *Global Change Biology*, *19*, 798–810.
Yuan, W., Liu, S., Yu, G., Bonnefond, J. M., Chen, J., Davis, K., et al. (2010). Global estimates of evapotranspiration and gross primary production based on MODIS and global meteorology data. *Remote Sensing of Environment*, *114*, 1416–1431.
Yuan, W., Liu, S., Zhou, G., Zhou, G., Tieszen, L. L., Baldocchi, D., et al. (2007). Deriving a light use efficiency model from eddy covariance flux data for predicting daily gross primary production across biomes. *Agricultural and Forest Meteorology*, *143*, 189–207.
Zhang, X., Friedl, M.A., Schaaf, C. B., Strahler, A. H., Hodges, J. C. F., Gao, F., et al. (2003). Monitoring vegetation phenology using MODIS. *Remote Sensing of Environment*, *84*, 471–475.
Zhang, J., Hu, Y., Xiao, X., Chen, P., Han, S., Song, G., et al. (2009). Satellite-based estimation of evapotranspiration of an old-growth temperate mixed forest. *Agricultural and Forest Meteorology*, *149*, 976–984.
Zhang, Y., Yu, Q., Jiang, J., & Tang, Y. (2008). Calibration of Terra/MODIS gross primary production over an irrigated cropland on the North China Plain and an alpine meadow on the Tibetan Plateau. *Global Change Biology*, *14*, 757–767.
Zhang, M., Yu, G., Zhuang, J., Gentry, R., Fu, Y., Sun, X., et al. (2011). Effects of cloudiness change on net ecosystem exchange, light use efficiency, and water use efficiency in typical ecosystems of China. *Agricultural and Forest Meteorology*, *151*, 803–816.